# Supporting Information

## Koch and Pillus 10.1073/pnas.0900809106

### SI Materials and Methods

**Plasmid Construction.** Plasmids described below are listed in Table S2. The plasmid pLP1951 was constructed by inserting the EagI *GAS1* fragment from YEpBS6 (pLP1823; gift from A. Conzelmann) (1) into pRS425 (pLP1623, 2$\mu$ *LEU2* vector). pLP2001 was obtained by direct PCR mutagenesis (2) of pLP1951 with oligonucleotides oLP818 and oLP819. pLP2002 was obtained by PCR mutagenesis of pLP1951 with oLP820 and oLP821. The plasmid pLP2114 was obtained by PCR mutagenesis of pLP2002 using the primers oLP818 and oLP819. The plasmids pLP2091, pLP2093, and pLP2094 resulted from ligating the SpeI-SacII fragment of pLP1951, pLP2001, and pLP2002 to SpeI-SacII digested pRS423 (pLP359, 2$\mu$ *HIS3* vector). pLP2117 was obtained by PCR mutagenesis on pLP2094 with oLP818 and oLP819. The plasmid pLP2087 was obtained by ligating the DraI fragment of pLP1951 to SmaI digested pGEX-4T-2 (pLP2057) to create an in-frame GST-tagged Gas1 construct. pLP2099 was obtained by PCR mutagenesis of pLP2087 using oLP820 and oLP821. pLP2119 was obtained by PCR mutagenesis of pLP2099 using oLP818 and oLP819. Oligonucleotides used for PCR mutagenesis are listed in Table S3.

**Immunoblot Analysis.** Levels of Sir2, Sir3, tubulin, acetylated histone H3K9/K14, acetylated histone H4K5, acetylated H4K16, and histone H3 were evaluated by immunoblot analysis as described (3). Cell extracts from 0.5 $A_{600}$ cell equivalents were separated on 18% (histones), 10% (tubulin), 9% (Sir2), or 8% (Sir3) SDS-polyacrylamide gels. Sir2 was detected using a 1:5,000 dilution of anti-Sir2 (4). Sir3 was detected using a 1:5,000 dilution of anti-Sir3 (3). Tubulin was detected using a 1:10,000 dilution of anti-$\beta$-tubulin (5). Acetylated H3K9/K14 (AcH3K9/K14) was detected using a 1:2,000 dilution of a polyclonal antiserum to acetylated H3K9/K14 (Millipore Corp.). Acetylated H4K5 (AcH4K5) was detected using a 1:2,000 dilution of a polyclonal antiserum to acetylated H4K5 (Serotec). Acetylated H4K16 (AcH4K16) was detected using a 1:2,000 dilution of a polyclonal antiserum to acetylated H4K16 (Millipore Corp.). Histone H3 was detected using a 1:10,000 dilution of a polyclonal antiserum to the C terminus of histone H3 (Millipore Corp.). Horseradish peroxidase-coupled anti-rabbit secondary antibody (Promega Corp.) was used at 1:10,000, and immunoblots were developed using ECL-Plus (GE Healthcare). Images of blots developed with ECL Plus were captured on the Typhoon Trio Variable Mode Imager (GE Healthcare) and analyzed using ImageQuant TL software.

**Fluorescence Microscopy.** Cells were grown in YPD to log phase ($A_{600}$ of 0.5–0.8), and DAPI was then added to a concentration of 2 $\mu$g/mL for 1 h at 30 °C. Cells were washed twice with PBS before imaging. Cells were visualized using an Axiovert 200M microscope (Carl Zeiss MicroImaging, Inc.) with a 100 × 1.3 NA objective. Images were captured using a monochrome digital camera (Axiocam; Carl Zeiss MicroImaging, Inc.). GFP images were deconvolved from 3 original stacks using Axiovision software (Carl Zeiss MicroImaging, Inc.).

**$NAD^+$ Hydrolysis Assays.** GST (GST; pLP1302), GST-Sir2 (pLP1275), GST-Gas1 (pLP2087), and GST-gas1-E161Q E262Q (pLP2119) fusion proteins were expressed in *E. coli* BL21 (DE3) during a 4- to 5-h induction with 0.5 mM IPTG at room temperature (for GST and Sir2) or 18 °C (for Gas1). Proteins were purified on glutathione Sepharose beads as directed (GE Healthcare). Purified proteins were dialyzed against 50 mM sodium phosphate (pH 7.2) and stored at 4 °C in 50 mM sodium phosphate (pH 7.2), 0.5 mM DTT (DTT), and 10% glycerol (6). Protein concentration was established by comparison of Coomassie Brilliant Blue (CBB) staining of purified GST protein samples and a concentration series of the BSA protein standard. $NAD^+$ hydrolysis assays to measure histone deacetylation were performed as described (7). Reactions were carried out in 1 mL with 50 mM sodium acetate (pH 5.5), 0.5 mM DTT, 5 mM tetrasodium pyrophosphate ($Na_4P_2O_7$), 0.1 mg/mL BSA, 1 mg calf thymus histones (Sigma) that were chemically acetylated (8), with 2 $\mu$Ci [4-$^3$H] $NAD^+$ (GE Healthcare; TRA298; 4.3 Ci/mmol, 1 mCi/mL), and 1.85 $\mu$g of purified proteins. The reactions were performed in duplicate and incubated at room temperature. Time points at 10 min, 45 min, 2 h, 3 h, and 5 h were taken by transfer of 185 $\mu$L of the reaction to tubes containing 135 $\mu$L 0.5 M boric acid (pH 8.0) to quench the reaction. One milliliter of ethyl acetate was added and vortexed for 5 min, and 700 $\mu$L of the ethyl acetate phase was transferred to 3 mL Ecoscint fluid (National Diagnostics) and analyzed by scintillation counting. Radioactivity released from Sir2 wild-type control reactions lacking histones was subtracted to establish values in Fig. S4*C*.


1. Vai M, Gatti E, Lacana E, Popolo L, Alberghina L (1991) Isolation and deduced amino acid sequence of the gene encoding gp115, a yeast glycophospholipid-anchored protein containing a serine-rich region. *J Biol Chem* 266:12242–12248.
2. Wang W, Malcolm BA (1999) Two-stage PCR protocol allowing introduction of multiple mutations, deletions and insertions using QuikChange site-directed mutagenesis. *Biotechniques* 26:680–682.
3. Stone EM, Pillus L (1996) Activation of an MAP kinase cascade leads to Sir3p hyperphosphorylation and strengthens transcriptional silencing. *J Cell Biol* 135:571–583.
4. Rusche LN, Kirchmaier AL, Rine J (2002) Ordered nucleation and spreading of silenced chromatin in *Saccharomyces cerevisiae*. *Mol Biol Cell* 13:2207–2222.
5. Bond JF, Fridovich-Keil JL, Pillus L, Mulligan RC, Solomon F (1986) A chicken-yeast chimeric beta-tubulin protein is incorporated into mouse microtubules in vivo. *Cell* 44:461–468.
6. Landry J, et al. (2000) The silencing protein SIR2 and its homologs are NAD-dependent protein deacetylases. *Proc Natl Acad Sci USA* 97:5807–5811.
7. Landry J, Slama JT, Sternglanz R (2000) Role of NAD(+) in the deacetylase activity of the SIR2-like proteins. *Biochem Biophys Res Commun* 278:685–690.
8. Parsons XH, Garcia SN, Pillus L, Kadonaga JT (2003) Histone deacetylation by Sir2 generates a transcriptionally repressed nucleoprotein complex. *Proc Natl Acad Sci USA* 100:1609–1614.

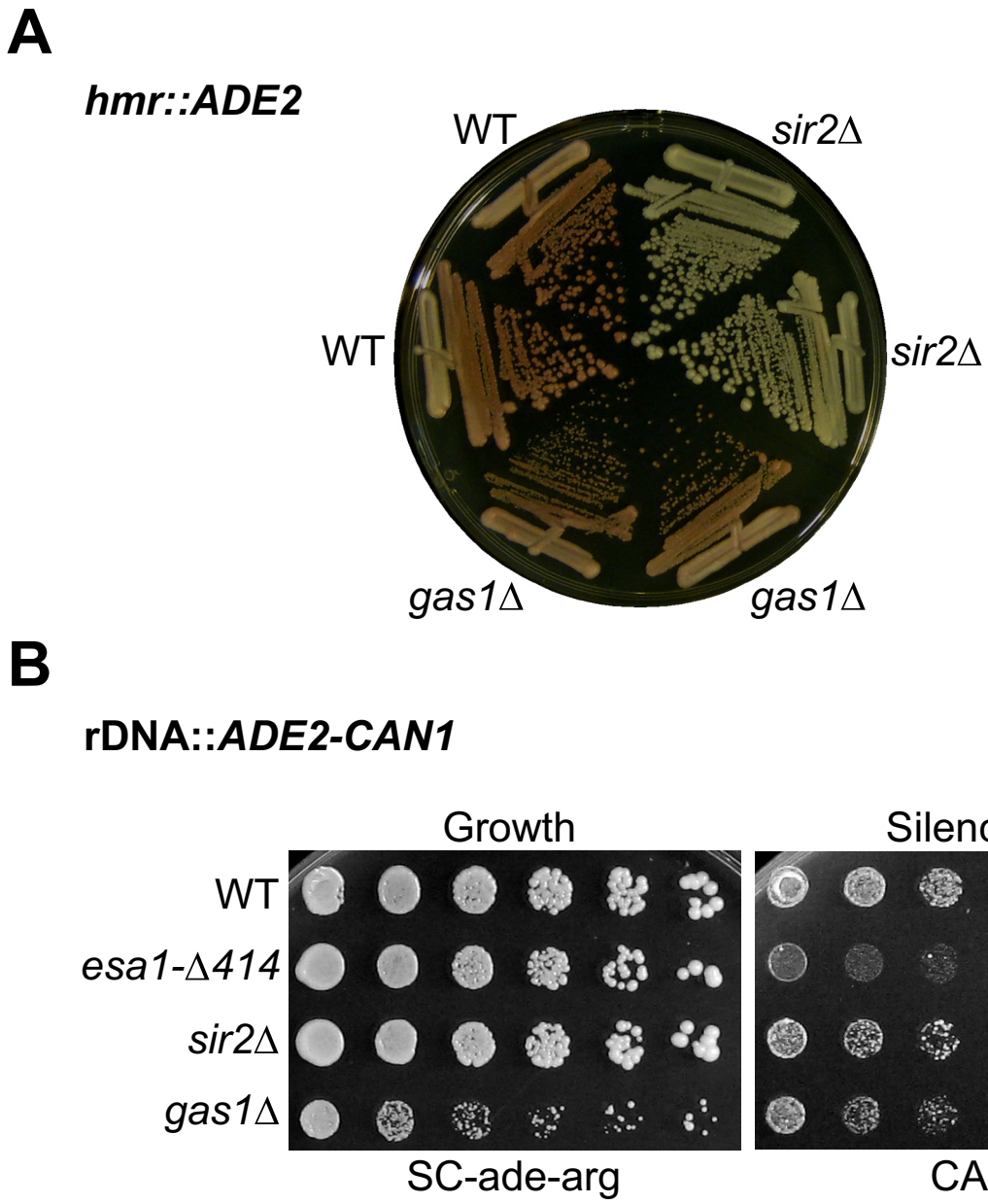


**Fig. S1.** Silencing of *HMR* and 25S rDNA is unaffected in *gas1*Δ mutants. (*A*) Deletion of *GAS1* does not affect *HMR* silencing. WT (LPY14324, LPY14235), *sir2*Δ (LPY11551, LPY11552), and *gas1*Δ (LPY14328, LPY14329) strains with a *hmr*::*ADE2* reporter in the context of a wild-type silencer (1) were struck on a YPD plate and incubated at 30 °C for 4 days. Plate was placed at 4 °C for 4 days before image capture. Note smaller colony formation of *gas1*Δ cells, representative of their growth defect. White colony color (*ADE2* expression) indicates defective silencing. Complete repression of *ADE2* gives rise to pink colonies. (*B*) rDNA silencing at the 25S locus is not enhanced in *gas1*Δ mutants. WT (LPY4908), *esa1-Δ414* (LPY4910), *sir2*Δ (LPY4978), and *gas1*Δ (LPY14408) strains with a rDNA::*ADE2-CAN1* reporter at 25S (2) (see Fig. 3*A* for location of reporter in rDNA) were plated on SC plates lacking adenine and arginine (SC-ade-arg) to monitor growth and SC-ade-arg containing 32 μg/mL canavanine (CAN) to monitor silencing. Decreased growth on canavanine plate indicates defective silencing. Note that the wild-type and *sir2*Δ strains show silencing of the reporter gene, whereas the *esa1-Δ414* mutant displays a prominent defect in silencing. *ESA1* contributes significantly to 25S rDNA silencing, whereas *SIR2*'s contribution is negligible (3). This is consistent with the observation that different genes have different contributions to rDNA silencing, depending on the location of the reporter. For *gas1*Δ, in contrast to the reporter at the 5S rDNA (Fig. 1*C*), there is no increase in silencing for this 25S reporter. Note that in this control plating, *gas1*Δ growth is reduced therefore the observation that its growth is comparable to *sir2*Δ on the canavanine plate underscores the conclusion that there is no influence on silencing at this locus.

1. Sussel L, Vannier D, Shore D (1993) Epigenetic switching of transcriptional states: Cis- and trans-acting factors affecting establishment of silencing at the *HMR* locus in *Saccharomyces cerevisiae*. *Mol Cell Biol* 13:3919–3928.
2. Fritze CE, Verschueren K, Strich R, Easton Esposito R (1997) Direct evidence for *SIR2* modulation of chromatin structure in yeast rDNA. *EMBO J* 16:6495–6509.
3. Clarke AS, Samal E, Pillus L (2006) Distinct roles for the essential MYST family HAT Esa1p in transcriptional silencing. *Mol Biol Cell* 17:1744–1757.

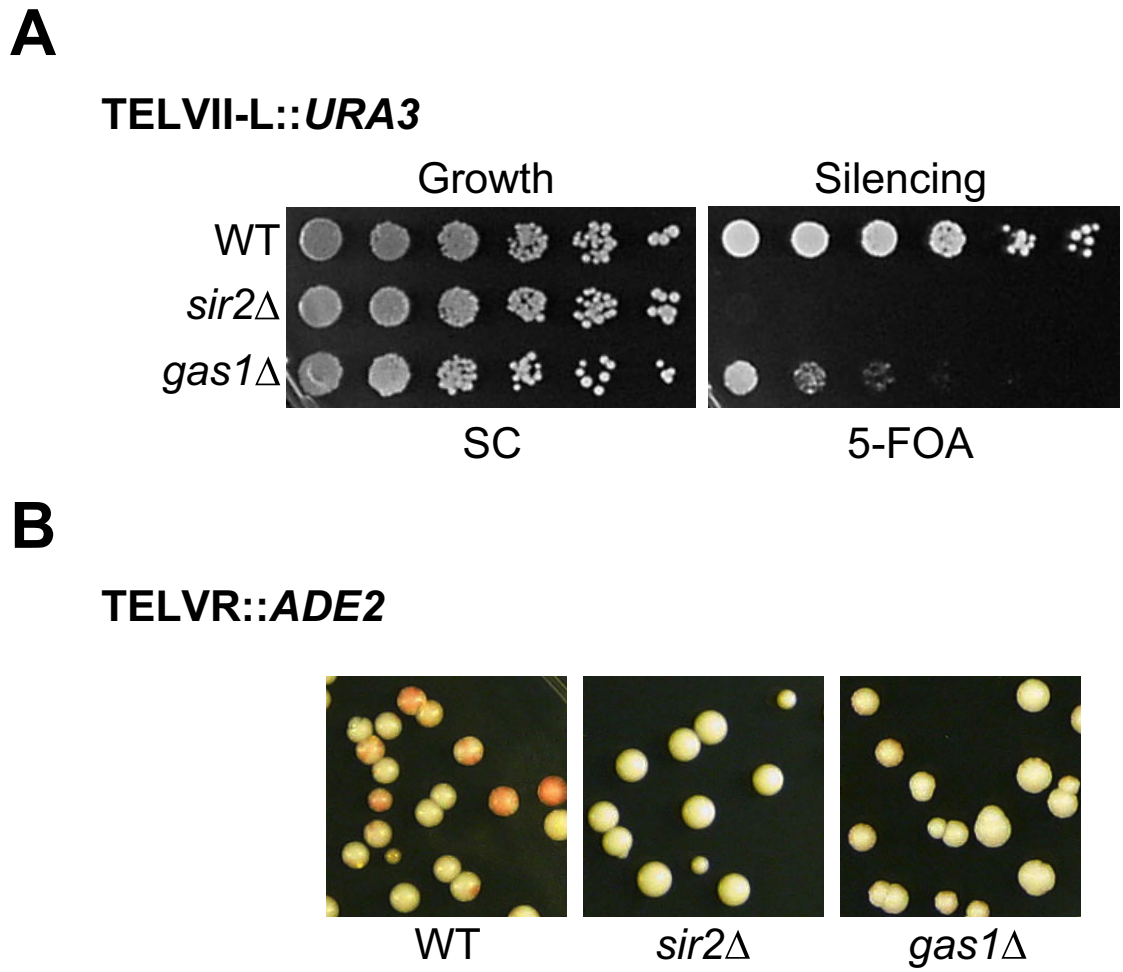


**Fig. S2.** The *gas1*Δ telomeric silencing defect is not telomere or promoter specific. (*A*) The *gas1*Δ telomeric silencing defect is observed at chromosome VII-L. WT (LPY1029), *sir2*Δ (LPY12660), and *gas1*Δ (LPY10358) strains with the *URA3* telomeric reporter on chromosome VII-L (1) were plated on SC to assay growth and SC containing 5-FOA to assay silencing. Decreased growth on 5-FOA indicates defective silencing. (*B*) The *gas1*Δ telomeric silencing defect is observed with a chromosome V-R *ADE2* telomeric reporter. WT (LPY9911), *sir2*Δ (LPY9961), and *gas1*Δ (LPY14400) strains were grown in YPD overnight and plated for single colonies on YPD. WT and *sir2*Δ plates were incubated at 30 °C for 3 days, and *gas1*Δ plates for 5 days. Plates were placed at 4 °C for 1 month, for red/pink color development, before image capture. White colony color (*ADE2* expression) indicates defective silencing.

1. Chien CT, Buck S, Sternglanz R, Shore D(1993) Targeting of Sir1 protein establishes transcriptional silencing at *HM* loci and telomeres in yeast. *Cell* 75:531–541.

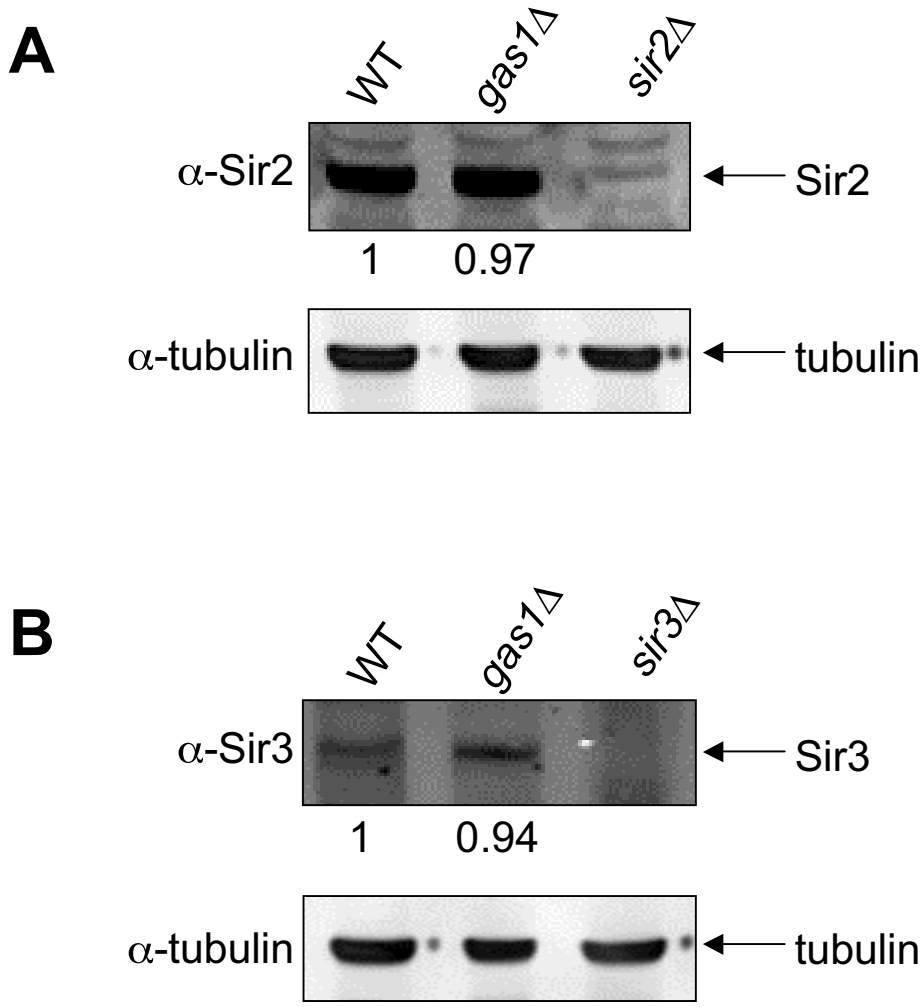


**Fig. S3.** Sir2 and Sir3 levels are unchanged in *gas1*Δ mutants. (*A*) Sir2 levels are unaltered in *gas1*Δ mutants. Whole-cell protein extracts from WT (LPY5), *gas1*Δ (LPY10129), and *sir2*Δ (LPY11) strains were separated by SDS-PAGE. Immunoblot analysis of Sir2 (65 kDa) was performed with anti-Sir2. Immunoblot analysis of tubulin (50 kDa) was performed with anti-β-tubulin. Images were captured on the Typhoon Trio Variable Mode Imager (GE Healthcare) and analyzed using ImageQuant TL software. Quantification with normalization to amount of tubulin is shown below Sir2 image, with WT set to 1. (*B*) Sir3 levels are unaltered in *gas1*Δ mutants. Whole-cell protein extracts from WT (LPY5), *gas1*Δ (LPY10129), and *sir3*Δ (LPY10) strains were separated by SDS-PAGE. Immunoblot analysis of Sir3 (116 kDa) was performed with anti-Sir3. Immunoblot analysis of tubulin (50 kDa) was performed with anti-β-tubulin. Images were captured as in *A*. Quantification with normalization to amount of tubulin is shown below Sir3 image, with WT set to 1.

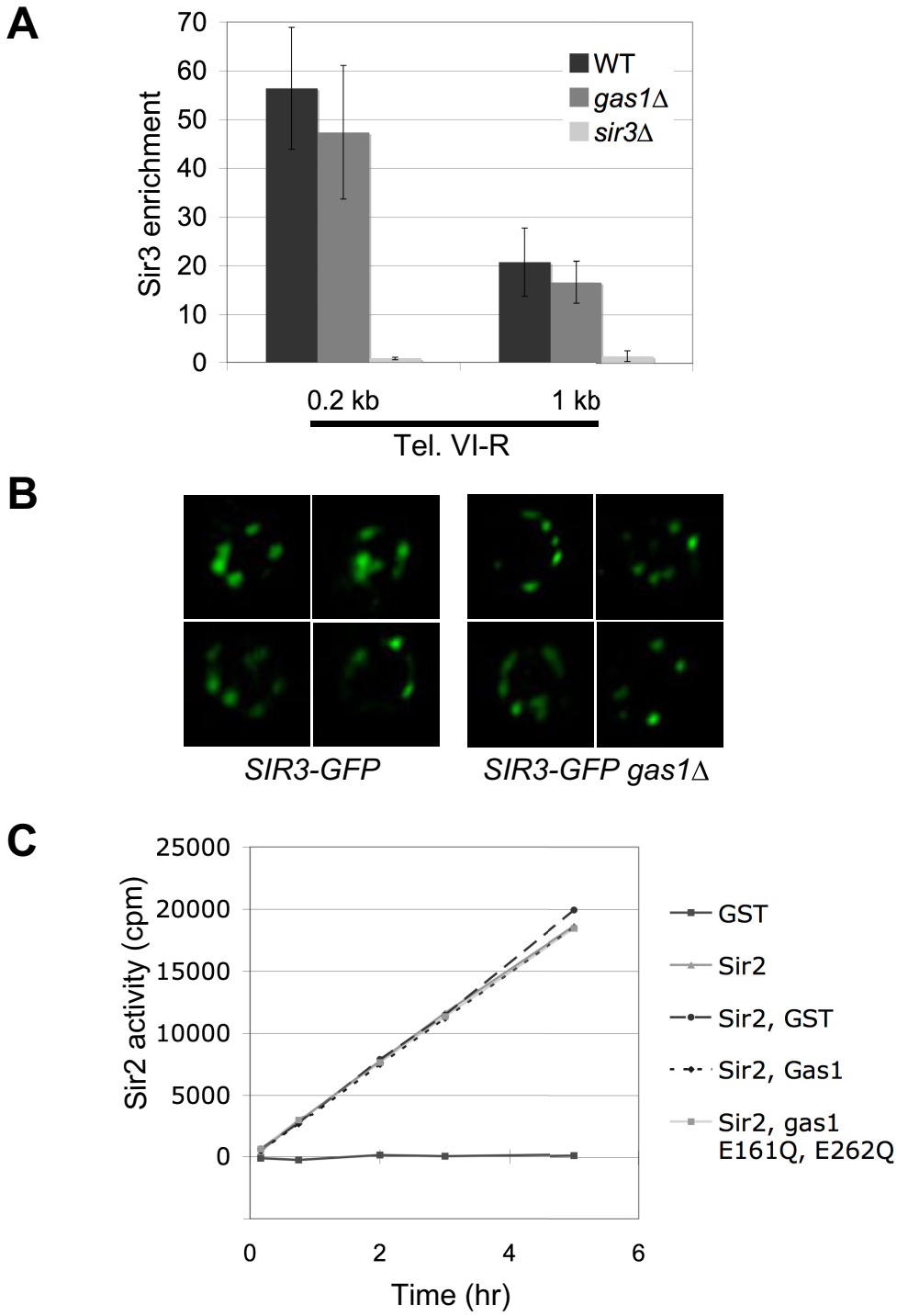


**Fig. S4.** Sir3 binds to the telomere and localizes to telomeric foci in *gas1*Δ; the in vitro histone deacetylase activity of Sir2 is unaffected by Gas1. (*A*) Levels of Sir3 occupancy in *gas1*Δ strains overlap those of wild-type cells at the telomere. ChIP of Sir3 was done in WT (LPY5), *sir3*Δ (LPY10), and *gas1*Δ (LPY10129) strains. Input and IP DNA were analyzed with primers shown in Fig. 3*A* and the nonspecific locus *ACT1*. Sir3 enrichment at the telomere was normalized to *ACT1*. (B) GFP-Sir3 localizes to telomeric foci in *gas1*Δ mutants. GFP-Sir3 was visualized in live cells in wild-type diploid (LPY12401) and *gas1*Δ diploid (LPY12462) strains. Three-dimensional deconvolution was used to resolve telomeric GFP-Sir3 foci. Each image is a representative nucleus containing GFP-Sir3 foci. (*C*) GST (pLP1302), GST-Sir2 (pLP1275), GST-Gas1 (pLP2087), and GST-Gas1 E161Q, E262Q (pLP2119) were expressed in and purified from bacteria. Purified proteins were added to $NAD^+$ hydrolysis assays containing $^3$H-$NAD^+$. GST-Sir2 activity shown correlates with the conversion of $^3$H-$NAD^+$ to $^3$H-nicotinamide. Sir2 activity was monitored over a 5-h time period. Addition of wild-type Gas1 or enzymatically inactive Gas1 to these assays neither enhanced nor inhibited Sir2 deacetylase activity.

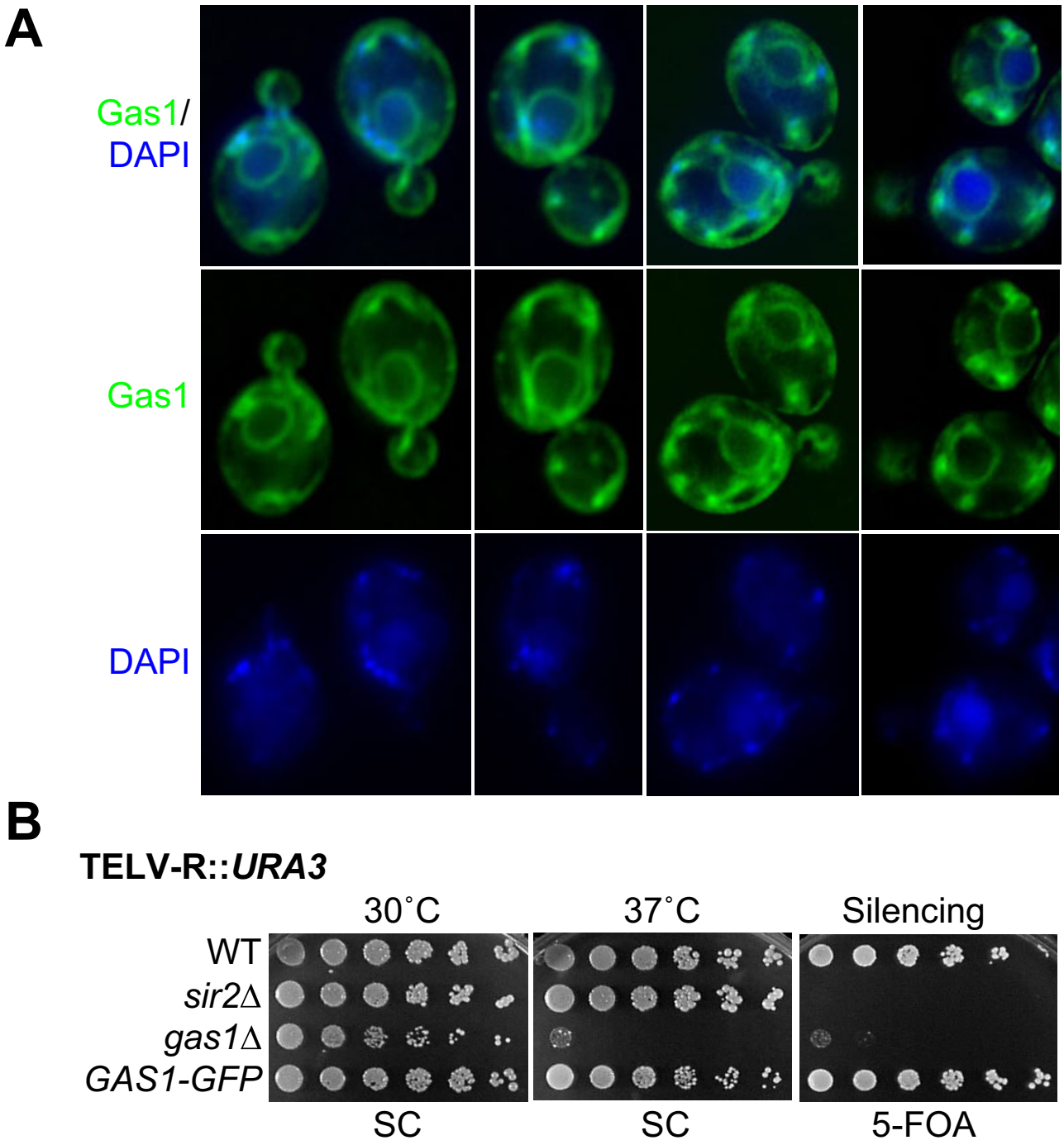


**Fig. S5.** GFP-Gas1 localizes to the nuclear periphery and is functional in telomeric silencing. (*A*) GFP-Gas1 localizes to the nuclear periphery. GFP-Gas1 (green) was visualized in live wild-type diploid cells (LPY14311). DNA was stained with DAPI (blue). Images shown are representative of nonbudded and budding cells. (*B*) *GAS1-GFP* functions in telomeric silencing. WT (LPY4916), *sir2*Δ (LPY10397), *gas1*Δ (LPY10362), and *GAS1-GFP* (LPY13691) with a *URA3* telomeric reporter on chromosome V-R were assayed for silencing as in Fig. 1*D*. To monitor growth (SC) and silencing (5-FOA), plates were incubated at 30 °C, and to monitor temperature sensitivity on SC, plates were incubated at 37 °C.

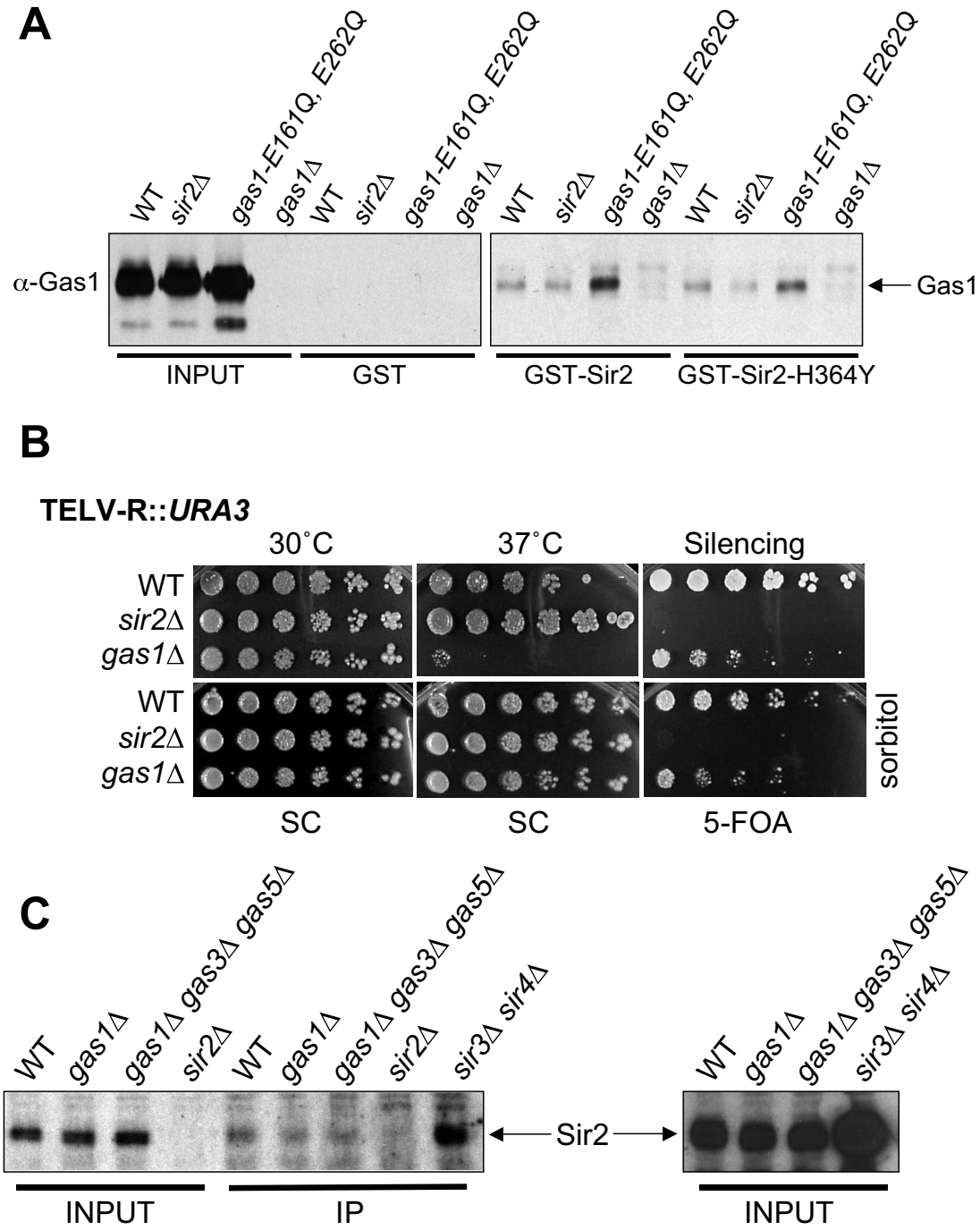


**Fig. S6.** Catalytically inactive versions of Sir2 and Gas1 interact by GST pulldown; *GAS1* function in telomeric silencing is separable from its role at the cell wall; Sir2 is immunoprecipitated by anti-β-1,3-glucan in *sir3*Δ *sir4*Δ strains. (*A*) sir2-H364Y and gas1-E161Q, E262Q physically interact by GST pull-down. GST (pLP1302), GST-Sir2 (pLP1275), and GST-sir2-H364Y (pLP1276) were purified and incubated with whole-cell extracts from WT (LPY5), *sir2*Δ (LPY11), *gas1-E161Q, E262Q* (LPY12251), and *gas1*Δ (LPY10129) strains. Bound protein was analyzed by immunobloting for Gas1 (125 kDa). (*B*) Sorbitol addition to growth medium suppresses *gas1*Δ temperature sensitivity but does not affect *gas1*Δ telomeric silencing. WT, *sir2*Δ, and *gas1*Δ strains used in Fig. S5*B* were plated on SC, with and without 1 M sorbitol, to assay growth at 30 °C and growth at elevated temperature (37 °C). 5-FOA plates, with and without 1 M sorbitol, were used to assay silencing at 30 °C. (*C*) β-1,3-glucan immunoprecipitations were performed in extracts from wild-type (LPY5), *gas1*Δ (LPY10129), *gas1*Δ *gas3*Δ *gas5*Δ (LPY13543), *sir3*Δ *sir4*Δ (LPY12625) strains overexpressing *SIR2* (pLP349) and from *sir2*Δ (LPY11) expressing a vector construct (pLP135). Transformed strains are LPY13545, LPY13549, LPY13553, LPY13653, and LPY13546, respectively. Immunoprecipitated material was analyzed by immunoblot for Sir2 (65 kDa). (*Right*) Separate immunoblot comparing input levels from *sir3*Δ *sir4*Δ srains to the other strains expressing *SIR2*. Note that input levels of Sir2 are elevated in *sir3*Δ *sir4*Δ, which is likely to result in the increased signal observed in the IP for the *sir3*Δ *sir4*Δ strain.

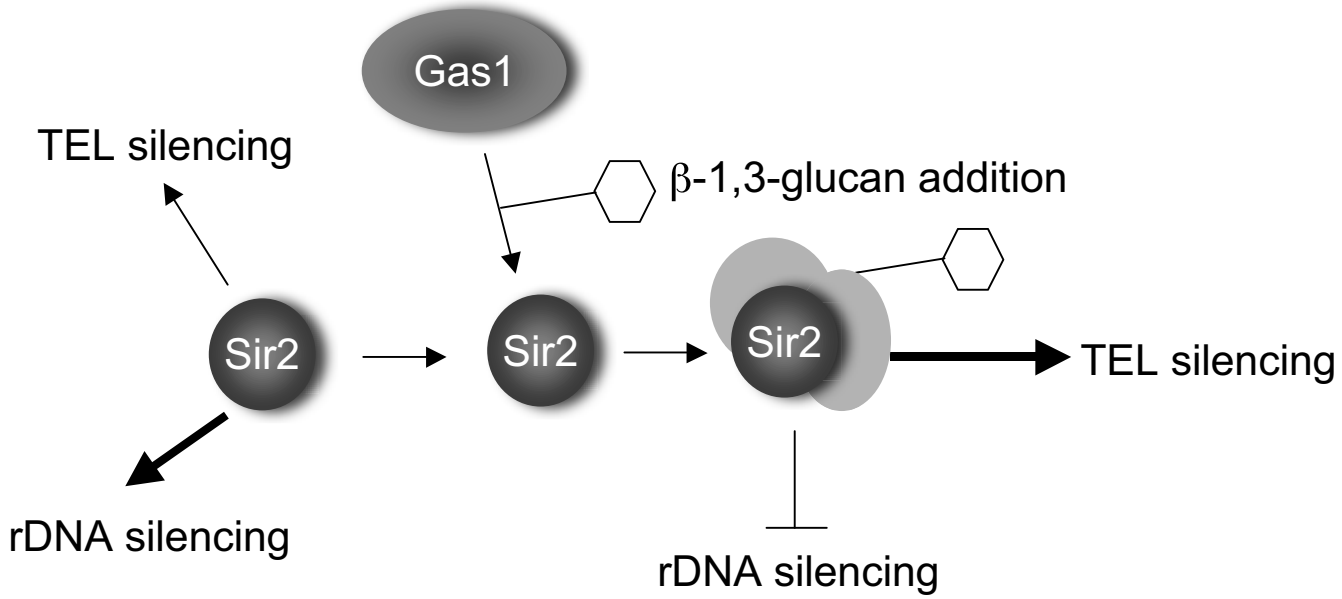


**Fig. S7.** A model summarizing Gas1 effects on transcriptional silencing. In wild-type cells, Sir2 functions in robust silencing of the rDNA. In the absence of Gas1 nuclear function, Sir2 can also weakly contribute to telomeric silencing. Gas1 physically interacts with Sir2 to alter the $\beta$-1,3-glucan modification state of Sir2, or other chromatin factors that Sir2 contacts, thereby strengthening Sir2 function in telomeric silencing and inhibiting Sir2 function in rDNA silencing. When *GAS1* function is lost, the modification to Sir2 (or other factors) is also lost, resulting in decreased telomeric silencing and increased rDNA silencing. Note that $\beta$-1,3-glucan is modeled as a single residue here (hexagon), yet Gas1 contributes to both $\beta$-1,3-glucan chain elongation and branching. The structure of any carbohydrate modification is likely to be more complex than that modeled here (1).

1. Popolo L, Vai M (1999) The Gas1 glycoprotein, a putative wall polymer cross-linker. *Biochim Biophys Acta* 1426:385–400.

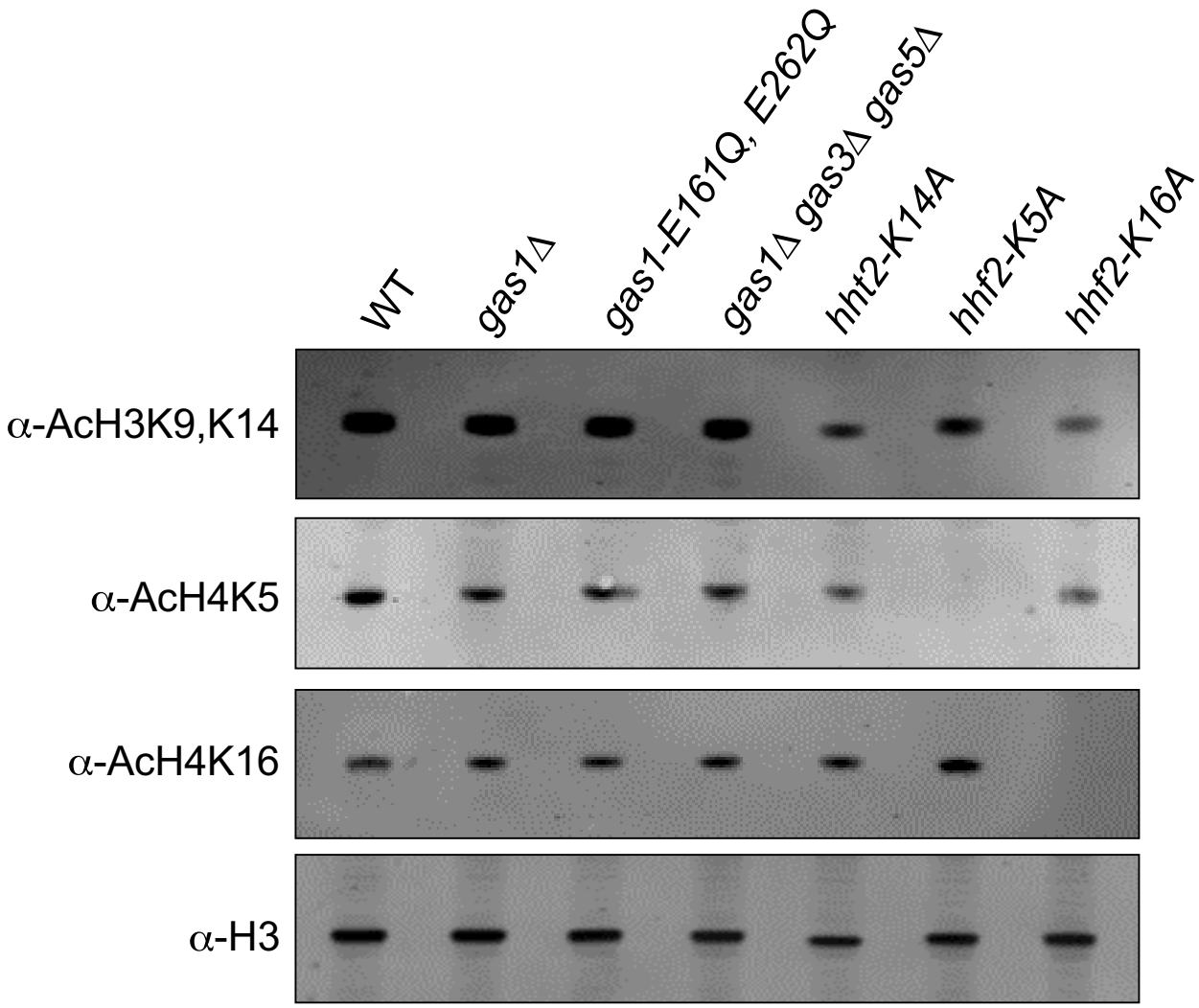


**Fig. S8.** Genome-wide acetylation of histone H3K9/K14, H4K5, and H4K16 is not controlled by *GAS1*. Whole-cell protein extracts from WT (LPY5), *gas1*Δ (LPY10129), *gas1-E161Q, E262Q* (LPY12251), *gas1*Δ *gas3*Δ *gas5*Δ (LPY13543), *hht2-K14A* (LPY13654), *hhf2-K5A* (LPY13656), and *hhf2-K16A* (LPY11509) were separated by SDS-PAGE. Immunoblot analysis was performed with antiserum specific to acetylated H3K9/K14 (AcH3K9/K14), acetylated H4K5 (AcH4K5), acetylated H4K16 (AcH4K16), and the C terminus of histone H3. Images were captured on the Typhoon Trio Variable Mode Imager (GE Healthcare).

**Table S1. Yeast strains used in this study**

| Strain (alias) | Genotype | Source/reference |
|---|---|---|
| LPY5 (W303–1a) | *MAT*a *ade2–1 can1–100 his3–11,15 leu2–3,112 trp1–1 ura3–1* | R. Rothstein |
| LPY10 | W303–1a *sir3*::*TRP1* | |
| LPY11 | W303–1a *sir2*::*HIS3* | |
| LPY79 (W303–1b) | *MAT*α *ade2–1 can1–100 his3–11,15 leu2,3,112 trp1–1 ura3–1* | R. Rothstein |
| LPY1029 (YDS631) | W303–1b *adh4*::*URA3*-$(C_{1-3}A)_n$ | (1) |
| LPY2446 (JS128) | *MAT*α *his3Δ200 leu2Δ1 ura3–167 RDN*::*Ty1-mURA3* | (2) |
| LPY2447 (JS163) | *MAT*α *his3Δ200 leu2Δ1 ura3–167 sir2Δ2*::*HIS3 RDN*::*Ty1-mURA3* | (3) |
| LPY3374 (PJ69–4A) | *MAT*a *gal4Δ gal80Δ his3–200 leu2–3,112 trp1–901 ura3–52 GAL2-ADE2 LYS2*::*GAL1-HIS3 met2*::*GAL7-lacZ* | (4) |
| LPY4908 | W303–1a rDNA::*ADE2-CAN1* | |
| LPY4910 | W303–1a *esa1-Δ414* rDNA::*ADE2-CAN1* | |
| LPY4912 | W303–1a *hmrΔE*::*TRP1* | |
| LPY4916 | W303–1a TELVR::*URA3* | |
| LPY4958 | W303–1a *sir1*::*LEU2 hmrΔE*::*TRP1* | |
| LPY4978 | W303–1b *sir2*::*HIS3* rDNA::*ADE2-CAN1* | |
| LPY4980 | W303–1a *sir2*::*HIS3 hmrΔE*::*TRP1* | |
| LPY7251 | LPY3374 + pLP956, pLP1205 | |
| LPY7252 | LPY3374 + pLP1073, pLP1205 | |
| LPY7253 | LPY3374 + pLP1074, pLP1205 | |
| LPY9046 | W303–1a *hht1-hhf1Δ*::*kanMX hht2-hhf2Δ*::*kanMX hta2-htb2Δ*::*HPH* + pJH33 | |
| LPY9911 | W303–1a TELVR::*ADE2* | |
| LPY9961 | W303–1b *sir2*::*HIS3* TELVR::*ADE2* | |
| LPY10074 | *MAT*α *his3Δ200 leu2Δ1 ura3–167 gas1Δ*::*kanMX RDN*::*Ty-1-mURA3* | |
| LPY10078 | *MAT*α *his3Δ200 leu2Δ1 ura3–167 gas1Δ*::*kanMX sir2Δ2*::*HIS3 RDN*::*Ty-1-mURA3* | |
| LPY10129 | W303–1a *gas1Δ*::*kanMX* | |
| LPY10358 | W303–1a *gas1Δ*::*kanMX trp1Δ0 ura3Δ0 adh4*::*URA3-UAS*$_G$ | |
| LPY10362 | W303–1a *gas1Δ*::*kanMX* TELVR::*URA3* | |
| LPY10397 | W303–1a *sir2*::*HIS3* TELVR::*URA3* | |
| LPY11509 | LPY9046 + pLP1990 | |
| LPY11551 | W303–1a *sir2*::*HIS3 hmr*::*ADE2* | |
| LPY11552 | W303–1b *sir2*::*HIS3 hmr*::*ADE2* | |
| LPY12232 | W303–1a *hht1-hhf1Δ*::*kanMX hht2-hhf2Δ*::*kanMX hta2-htb2Δ*::*HPH* + pJH33 | |
| LPY12251 | LPY10129 + pLP2114 | |
| LPY12337 | W303–1a *gas3Δ*::*kanMX* TELVR::*URA3* | |
| LPY12348 | W303–1a *gas5Δ*::*kanMX* TELVR::*URA3* | |
| LPY12401 | *MATa/MAT*α *his3Δ1/his3Δ1 leu2Δ0/leu2Δ0 LYS2/LYS2 met15Δ0/met15Δ0 ura3Δ0/ura3Δ0 GFP-SIR3-HIS3MX6/GFP-SIR3-HIS3MX6* | |
| LPY12462 | *MATa/MAT*α *his3Δ1/his3Δ1 leu2Δ0/leu2Δ0 lys2Δ0/LYS2 MET15/met15Δ0 ura3Δ0/ura3Δ0 GFP-SIR3-HIS3MX6/GFP-SIR3-HIS3MX6 gas1Δ*::*kanMX/gas1Δ*::*kanMX* | |
| LPY12625 | W303–1b *sir3*::*TRP1 sir4*::*HIS3* | |
| LPY12660 | W303–1b *sir2*::*HIS3 ura3Δ0 adh4*::*URA3-UAS*$_G$ | |
| LPY13094 | W303–1a *bgl2Δ*::*kanMX* TELVR::*URA3* | |
| LPY13166 | LPY9046 + pLP2282 (pFX05) | |
| LPY13543 | W303–1b *gas1Δ*::*kanMX gas3Δ*::*kanMX gas5Δ*::*kanMX* | |
| LPY13545 | LPY5 + pLP349 | |
| LPY13546 | LPY11 + pLP135 | |
| LPY13549 | LPY10129 + pLP349 | |
| LPY13553 | LPY13543 + pLP349 | |
| LPY13554 | LPY4916 + pLP359 | |
| LPY13559 | LPY4916 + pLP2091 | |
| LPY13562 | LPY4916 + pLP2117 | |
| LPY13563 | LPY10362 + pLP359 | |
| LPY13568 | LPY10362 + pLP2091 | |
| LPY13569 | LPY10362 + pLP2093 | |
| LPY13570 | LPY10362 + pLP2094 | |
| LPY13571 | LPY10362 + pLP2117 | |
| LPY13653 | LPY12625 + pLP349 | |
| LPY13654 | LPY9046 + pLP1777 | |
| LPY13656 | LPY12232 + pLP2181 | |
| LPY13659 | W303–1b *hml*::*TRP1* | |
| LPY13660 | W303–1a *sir1*::*LEU2 hml*::*TRP1* | |
| LPY13661 | W303–1a *gas1Δ*::*kanMX hml*::*TRP1* | |
| LPY13665 | W303–1a *gas1Δ*::*kanMX hmrΔE*::*TRP1* | |

| Strain (alias) | Genotype | Source/reference |
|---|---|---|
| LPY13691 | *MAT*a *ade2–1 his3Δ1* or *his3–11,15 leu2Δ0* or *leu2–3,112 ura3Δ0* or *ura3–1GFP-GAS1-HIS3MX6*TELVR::*URA3* | |
| LPY14311 | *MAT*a/*MAT*α *his3Δ1/his3Δ1 leu2Δ0/leu2Δ0 LYS2/LYS2 met15Δ0/MET15 ura3Δ0/ura3Δ0 GFP-GAS1-HIS3MX6/GFP-GAS1-HIS3MX6* | |
| LPY14324 | W303–1a *hmr*::*ADE2* | |
| LPY14325 | W303–1b *hmr*::*ADE2* | |
| LPY14328 | W303–1a *gas1Δ*::*kanMX hmr*::*ADE2* | |
| LPY14329 | W303–1b *gas1Δ*::*kanMX hmr*::*ADE2* | |
| LPY14400 | W303–1a *gas1Δ*::*kanMX* TELVR::*ADE2* | |
| LPY14408 | W303–1b *gas1Δ*::*kanMX* rDNA::*ADE2-CAN1* | |

Unless otherwise noted, strains were constructed during the course of this study or are part of the standard lab collection.


1. Popolo L, Vai M (1999) The Gas1 glycoprotein, a putative wall polymer cross-linker. *Biochim Biophys Acta* 1426:385–400.
2. Smith JS, Brachmann CB, Pillus L, Boeke JD (1998) Distribution of a limited Sir2 protein pool regulates the strength of yeast rDNA silencing and is modulated by Sir4p. *Genetics* 149:1205–1219.
3. Sherman JM, *et al.* (1999) The conserved core of a human *SIR2* homologue functions in yeast silencing. *Mol Biol Cell* 10:3045–3059.
4. James P, Halladay J, Craig EA (1996) Genomic libraries and a host strain designed for highly efficient two-hybrid selection in yeast. *Genetics* 144:1425–1436.

**Table S2. Plasmids used in this study**

| Plasmid (alias) | Description | Source/reference |
|---|---|---|
| pLP135 (YEp351) | vector *LEU2* 2$\mu$ | (1) |
| pLP349 | *SIR2 LEU2* 2$\mu$ | (2) |
| pLP359 (pRS423) | vector *HIS3* 2$\mu$ | (3) |
| pLP956 (pGBD-C1) | GBD *TRP1* 2$\mu$ | (4) |
| pLP1073 | GBD-core *SIR2 TRP1* 2$\mu$ | (5) |
| pLP1074 | GBD-*SIR2 TRP1* 2$\mu$ | (5) |
| pLP1205 | GAD-*GAS1 LEU2* 2$\mu$ | (6) |
| pLP1275 (pDM111a) | GST-*SIR2* | (7) |
| pLP1276 (pDM360) | GST-*sir2-H364Y* | (7) |
| pLP1302 (pGEX-4T-1) | GST | (8) |
| pLP1623 (pRS425) | vector *LEU2* 2$\mu$ | (3) |
| pLP1777 | *HHF2 hht2-K14A TRP1* CEN | |
| pLP1823 (YEpBS6) | *GAS1 URA3* 2$\mu$ | (9) |
| pLP1951 | *GAS1 LEU2* 2$\mu$ | |
| pLP1990 | *hhf2-K16A HHT2 TRP1* CEN | |
| pLP2001 | *gas1-E161Q LEU2* 2$\mu$ | |
| pLP2002 | *gas1-E262Q LEU2* 2$\mu$ | |
| pLP2057 (pGEX-4T-2) | GST | (8) |
| pLP2087 | GST-*GAS1* | |
| pLP2091 | *GAS1 HIS3* 2$\mu$ | |
| pLP2093 | *gas1-E161Q HIS3* 2$\mu$ | |
| pLP2094 | *gas1-E262Q HIS3* 2$\mu$ | |
| pLP2099 | GST-*gas1-E262Q* | |
| pLP2114 | *gas1-E161Q E262Q LEU2* 2$\mu$ | |
| pLP2117 | *gas1-E161Q E262Q HIS3* 2$\mu$ | |
| pLP2119 | GST-*gas1-E161Q E262Q* | |
| pLP2181 | *hhf2-K5A HHT2 TRP1* CEN | |
| pLP2282 (pFX05) | *HHF2 hht2-K56Q TRP1* CEN | (10) |

Unless otherwise noted, plasmids were constructed during the course of this study (see *SI Materials and Methods*) or are part of the standard lab collection.


1. Hill JE, Myers AM, Koerner TJ, Tzagoloff A (1986) Yeast/E. coli shuttle vectors with multiple unique restriction sites. *Yeast* 2:163–167.
2. Sherman JM, *et al.* (1999) The conserved core of a human *SIR2* homologue functions in yeast silencing. *Mol Biol Cell* 10:3045–3059.
3. Christianson TW, Sikorski RS, Dante M, Shero JH, Hieter P (1992) Multifunctional yeast high-copy-number shuttle vectors. *Gene* 110:119–122.
4. James P, Halladay J, Craig EA (1996) Genomic libraries and a host strain designed for highly efficient two-hybrid selection in yeast. *Genetics* 144:1425–1436.
5. Garcia SN, Pillus L (2002) A unique class of conditional *sir2* mutants displays distinct silencing defects in *Saccharomyces cerevisiae*. *Genetics* 162:721–736.
6. Garcia SN (2003) Ph.D. dissertation, (University of California at San Diego, La Jolla, CA), pp. 116–177.
7. Tanny JC, Dowd GJ, Huang J, Hilz H, Moazed D (1999) An enzymatic activity in the yeast Sir2 protein that is essential for gene silencing. *Cell* 99:735–745.
8. Kaelin WG, Jr, *et al.* (1992) Expression cloning of a cDNA encoding a retinoblastoma-binding protein with E2F-like properties. *Cell* 70:351–364.
9. Vai M, Gatti E, Lacana E, Popolo L, Alberghina L (1991) Isolation and deduced amino acid sequence of the gene encoding gp115, a yeast glycophospholipid-anchored protein containing a serine-rich region. *J Biol Chem* 266:12242–12248.
10. Xu F, Zhang Q, Zhang K, Xie W, Grunstein M (2007) Sir2 deacetylates histone H3 lysine 56 to regulate telomeric heterochromatin structure in yeast. *Mol Cell* 27:890–900.

**Table S3. Oligonucleotide sequences used in this study**

| Oligo no. | Name | Sequence (5′ –3′ ) | Source/reference |
|---|---|---|---|
| oLP416 | *GAS1*-F2 | ATAAAGCGAGCTGGTGCCTATCATAGCCG | |
| oLP417 | *GAS1*-R2 | AATTGTGTGTGCTCAATCTAATATCTCCGC | |
| oLP675 | *GAS3*-F | TCTTTCTGCTGCGGAAGCGCTATACGGC | |
| oLP676 | *GAS3*-R | CCATGGCTCAAGGATCCCTTGGGTATGG | |
| oLP766 | TEL6R-1 kb-F | GGACCTACTAGTGTCTATAGTAAGTG | (1) |
| oLP767 | TEL6R-1 kb-R | CTCTAACATAACTTTGATCCTTACTCG | (1) |
| oLP774 | 25S-F | TGTTGAAAGGGAAGGGCATT | (2) |
| oLP775 | 25S-R | AGCAGAGGGCACAAAACACC | (2) |
| oLP776 | 5S-R | CATGGAGCAGTTTTTTCCGC | (2) |
| oLP777 | 5S-F | TACAAGCACTCATGTTTGCCG | (2) |
| oLP778 | TEL6R-0.2 kb-F | AAATGGCAAGGGTAAAAACCG | (2) |
| oLP779 | TEL6R-0.2 kb-R | TCGGATCACTACACACGGAAAT | (2) |
| oLP798 | *ACT1*-F1 | GGTGGTTCTATCTTGGCTTC | (1) |
| oLP799 | *ACT1*-R1 | ATGGACCACTTTCGTCGTAT | (1) |
| oLP815 | *GAS5*-F *Eag*I | CTTCGATCTGCGG**C**CGTTACTTCTAACG | |
| oLP816 | *GAS5*-R *Bam*HI | TGAGGAT**C**CAACTTCGATCTCATCAGCG | |
| oLP818 | *GAS1-E161Q*-F | GGTTTCTTCGCCGGTAAT**C**AAGTTACTAACAATTACACC | |
| oLP819 | *GAS1-E161Q*-R | GGTGTAATTGTTAGTAACTT**G**ATTACCGGCGAAGAAACC | |
| oLP820 | *GAS1-E262Q*-F | CCTGTTTTCTTCTCT**C**AATACGGTTGTAACG | |
| oLP821 | *GAS1-E262Q*-R | CGTTACAACCGTATT**G**AGAGAAGAAAACAGG | |
| oLP871 | INT-ChrV_sense | GTGTTTGACCCGAGGGTATG | F. Winston/V. Cheung |
| oLP872 | INT-ChrV_antisense | TAAGGTCCACACCGTCATCA | F. Winston/V. Cheung |
| oLP1010 | *BGL2*-F | CAGTGGTGACTTCCACTACG | |
| oLP1011 | *BGL2*-R | TGGACTACGAAACGGATGGC | |

Nucleotides in bold in the above sequences are mutagenic, compared with the wild-type sequence.

1. Darst RP, Garcia SN, Koch MR, Pillus L (2008) Slx5 promotes transcriptional silencing and is required for robust growth in the absence of Sir2. *Mol Cell Biol* 28:1361–1372.
2. Emre NC, *et al.* (2005) Maintenance of low histone ubiquitylation by Ubp10 correlates with telomere-proximal Sir2 association and gene silencing. *Mol Cell* 17:585–594.